ACS OMEGA

http://pubs.acs.org/journal/acsodf

Article

Green Synthesis of Zinc Oxide (ZnO) Nanoparticles Using Aqueous Fruit Extracts of *Myristica fragrans*: Their Characterizations and Biological and Environmental Applications

Shah Faisal,* Hasnain Jan, Sajjad Ali Shah, Sumaira Shah, Adnan Khan, Muhammad Taj Akbar, Muhammad Rizwan, Faheem Jan, Wajidullah, Noreen Akhtar, Aishma Khattak, and Suliman Syed

Cite This: *ACS Omega* 2021, 6, 9709−9722

Read Online

ACCESS | Metrics & More | Article Recommendations

ABSTRACT: In the present work, bioaugmented zinc oxide nanoparticles (ZnO-NPs) were prepared from aqueous fruit extracts of *Myristica fragrans*. The ZnO-NPs were characterized by different techniques such as X-ray diffraction (XRD), Fourier transform infrared (FTIR) spectroscopy, ultraviolet (UV) spectroscopy, scanning electron microscopy (SEM), transmission electron microscopy (TEM), dynamic light scattering (DLS), and thermogravimetric analysis (TGA). The crystallites exhibited a mean size of 41.23 nm measured via XRD and were highly pure, while SEM and TEM analyses of synthesized NPs confirmed their spherical or elliptical shape. The functional groups responsible for stabilizing and capping of ZnO-NPs were confirmed using FTIR analysis. The ζ-size and ζ-potential of synthesized ZnO-NPs were reported as 66 nm and −22.1 mV, respectively, via the DLS technique can be considered as moderate stable colloidal solution. Synthesized NPs were used to evaluate for their possible antibacterial, antidiabetic, antioxidant, antiparasitic, and larvicidal properties. The NPs were found to be highly active against bacterial strains both coated with antibiotics and alone. *Klebsiella pneumoniae* was found to be the most sensitive strain against NPs (27 ± 1.73) and against NPs coated with imipinem (26 ± 1.5). ZnO-NPs displayed outstanding inhibitory potential against enzymes protein kinase (12.23 ± 0.42), α-amylase (73.23 ± 0.42), and α-glucosidase (65.21 ± 0.49). Overall, the synthesized NPs have shown significant larvicidal activity (77.3 ± 1.8) against *Aedes aegypti*, the mosquitoes involved in the transmission of dengue fever. Similarly, tremendous leishmanicidal activity was also observed against both the promastigote (71.50 ± 0.70) and amastigote (61.41 ± 0.71) forms of the parasite. The biosynthesized NPs were found to be excellent antioxidant and biocompatible nanomaterials. Biosynthesized ZnO-NPs were also used as photocatalytic agents, resulting in 88% degradation of methylene blue dye in 140 min. Owing to their eco-friendly synthesis, nontoxicity, and biocompatible nature, ZnO-NPs synthesized from *M. fragrans* can be exploited as potential candidates for biomedical and environmental applications.

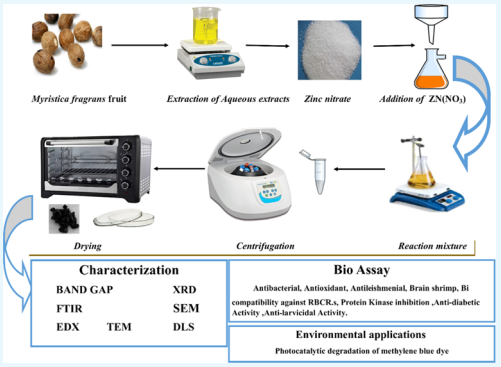

INTRODUCTION

Nanotechnology is now considered to be a proven state-of-the-art technology with numerous branches embedded in industrial fields such as chemical, pharmaceutical, mechanical, and food processing industries. Nanotechnology also plays an interesting role in the areas of computing, power generation, optics, drug delivery, and environmental sciences.[1] In the advent of nanotechnology, many nanoscale devices have been developed using numerous methods, such as physical, chemical, and green approaches. Yet, green nanoparticle synthesis is a tool of choice that can be easily prepared and engineered.[2] There are many drawbacks of conventional approaches for the synthesis of nanoparticles, including long-term processing, high cost, laborious procedures, and in particular the use of toxic compounds. Most of the relevant study has been directed to eco-friendly and fast synthesis protocols for the production of nanoparticles due to these limitations.[3,4] For material scientists, the development of eco-friendly methods for synthesizing nanoscale materials has been a major focus in recent years. In this respect, green synthesis of NPs, especially using extracts from different plants, is a growing trend that is considered simple, cheap, and nontoxic in green chemistry.[5−7] Nanotechnology has also increased the human standard of living by addressing many everyday life issues, such as the contribution to energy sufficiency; climate

Received: January 18, 2021
Accepted: March 15, 2021
Published: March 30, 2021

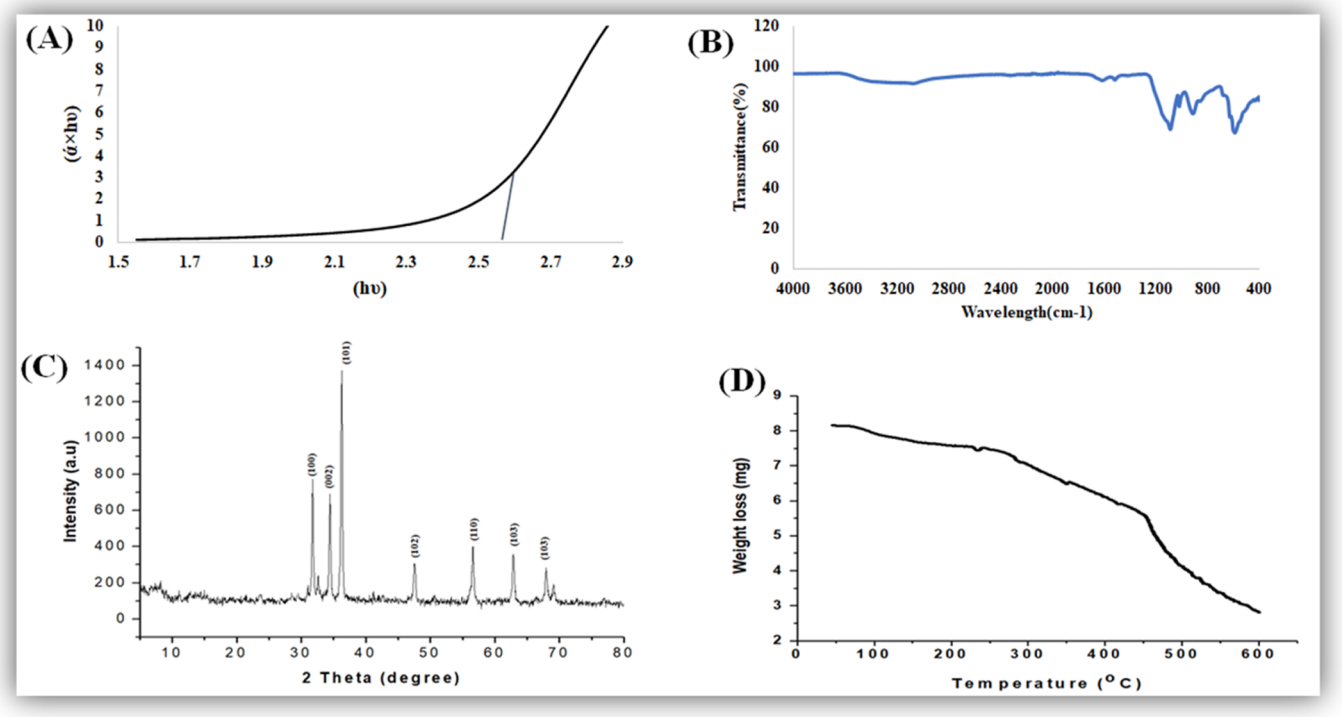

Figure 1. (A) UV band gap, (B) typical FTIR spectra, (C) typical XRD pattern, and (D) typical TGA pattern of *M. fragrans* fruit-synthesized ZnO-NPs.

change; beauty, textile, and health industries including the cure of deadly diseases such as cancers and Alzheimer's.[8,9]

Due to their multiple applications in various technical fields, comprehensive investigation into metal oxide nanoparticles has been concentrated in the past decade.[10] Among these, with multifaceted benefits, ZnO-NPs are exciting inorganic materials. ZnO-NPs can be used in various sectors, such as energy conservation, textiles, electronics, healthcare, catalysis, cosmetics, semiconductors, and chemical sensing.[11−15] The NPs are nontoxic and biocompatible and display excellent biomedical applications, such as anticancer,[16] anti-inflammatory,[17] and antimicrobial properties, in targeted drug delivery,[18] wound healing, and bioimaging.[19,20]

Nanoproducts can be produced from different methods (chemical, physical, and biosynthesis) with multiple properties and huge applications. Plant-based synthesis of ZnO-NPs has previously been reported though, inadequate literature is existing on their diverse biological properties such as antimicrobial, antilarvicidal, protein kinase, and anticancer activities. The curative uses of *Myristica fragrans* (Jaiphal) are well known, and it is mainly used as an anti-inflammatory, antidiarrheal, analgesic, and sex stimulanting agent.[21]

Here, we report plant-based synthesis of zinc oxide nanoparticles using the aqueous extracts of *M. fragrans* fruits. Green synthesis of ZnO-NPs has eco-friendly aspects and various biomedical applications. The metabolites found in the aqueous extract of *M. fragrans* act as an oxidizing, reducing, and capping agent for the synthesis of biogenic ZnO-NPs. The green synthesized nanoparticles will be characterized using modern techniques such as Fourier transform infrared (FTIR) spectroscopy, ultraviolet (UV) spectroscopy, X-ray diffraction (XRD), scanning electron microscopy (SEM), transmission electron microscopy (TEM), dynamic light scattering (DLS), and thermal gravimetric analysis (TGA). The NPs will be checked for their antimicrobial, antileishmanial, antidiabetic, antioxidant, antilarvicidal, and protein kinase inhibitory potential.

RESULTS AND DISCUSSION

Biosynthesis of ZnO-NPs. *M. fragrans* is known as "nutmeg"; its extracts and essential oils are important in drug development with numerous pharmacological activities in South Africa, India, and other tropical countries.[22] For a long time, *M. fragrans* has been used in traditional medicines as a carminative, stimulant, narcotic, emmenagogue, and abortifacient. Nutmeg is also prescribed for the treatment of many diseases, such as rheumatism, muscle spasm, decreased appetite, and diarrhea. *M. fragrans* has recently been shown to have antioxidant, anticonvulsant, analgesic, anti-inflammatory, antidiabetic, antibacterial, and antifungal activities. Trimyristin, myristic acid, myristicin, safrole, and elimicin are reported from nutmeg. Due to the easy collection of nutmeg, widespread presence, and also remarkable biological activities, it has become both food and medicine in tropical countries, especially in India and China.[22,23] The biosynthesis of zinc oxide nanoparticles was carried out using aqueous fruit extracts of *M. fragrans* as reducing, capping, and stabilizing agents.[24] Broad studies disclose that volatile oils are the major constituents within the dry biomass of *M. fragrans*. Among numerous constituents, D-pinene, myristin, and myristic acid and its esters contribute to the high percentage of the dry weight. Moreover, myristicin, fatty acids, and mesin constitute one-half of the dry biomass.[25−27] It is assumed that the constituents present in *M. fragrans* biomass have contributed a lot in the preparation of eco-friendly and biomedically important zinc oxide nanoparticles. When the reaction is carried out between $Zn(NO_3)_2{\cdot}2H_2O$ and *M. fragrans*, the color of the mixture changes from light brown to dark gray, which confirms the formation of zinc oxide nanoparticles

https://doi.org/10.1021/acsomega.1c00310
ACS Omega 2021, 6, 9709−9722

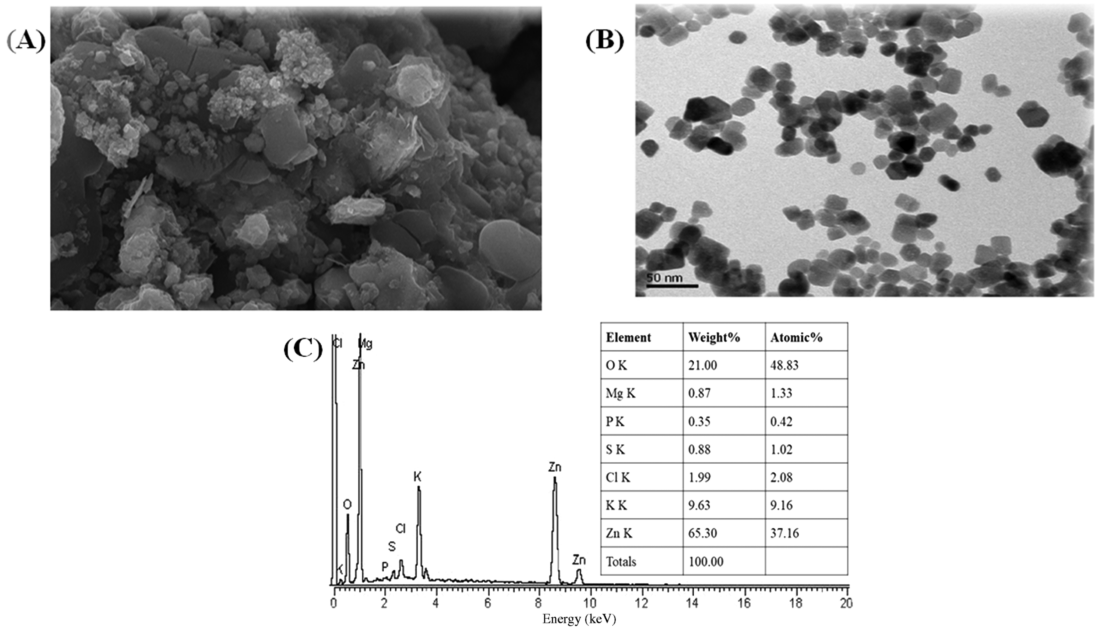

Element	Weight%	Atomic%
O K	21.00	48.83
Mg K	0.87	1.33
P K	0.35	0.42
S K	0.88	1.02
Cl K	1.99	2.08
K K	9.63	9.16
Zn K	65.30	37.16
Totals	100.00	

Figure 2. (A) SEM micrograph, (B) TEM micrograph, and (C) EDX spectrograph of *M. fragrans* fruit-synthesized ZnO-NPs.

(ZnO-NPs).[28] After subsequent steps of washing, drying, grinding, and calcination, white powder of ZnO-NPs was obtained. The fine powder collected was stored in an airtight glass vial, labeled as ZnO-NPs, at room temperature for physicochemical and morphological characterizations and biological applications. The literature study revealed that physicochemical and morphological characteristics of ZnO-NPs mainly depend on the type and species of plant used and the reaction conditions such as the pH, temperature, and synthesis medium.[29]

Band Gap. The band gap of ZnO-NPs is characterized by performing UV−visible spectroscopy. The particles show a very sharp band gap, which was 2.57 eV. The smaller band gap will easily categorize a photocatalytic reaction of the nanoparticles and show good photocatalytic activity for the degradation of methylene blue dye, as shown in Figure 1A. Because of the smaller band gap, the electron is easily excited from the valence band to the conduction band. In the previous literature, it was reported in ref 30 by performing UV spectroscopy on ZnO-NPs that the band gap obtained was 3.29 eV. The Tauc plot method was used to calculate the band gap, as shown in Figure 1A, which is very close to the value reported in the literature.[31,32] The band gap depends on various factors, including the grain size, oxygen deficiency, surface roughness, and lattice strain.[33]

Fourier Transform Infrared (FTIR) Spectroscopy. To classify functional groups in the aqueous extract and zinc oxide nanoparticles, we perform FTIR spectroscopy in the range of 4000−400 cm^{-1}, as shown in Figure 1B. The peak of ZnO obtained at 469 cm^{-1} could be due to zinc and oxygen bonding vibrations.[34] The low absorption peak observed at around 3420 and 3200 cm^{-1} could be appointed to hydroxyl (OH) groups; also, some other bands were observed at around 1600, 1100, and 900 cm^{-1}. A major change in IR spectra was noticed in this range. A deep absorbance band at 1100 indicates the presence of carbohydrate (C−O), (C═C) rings (polysaccharides, pectin, and cellulose). Both primary and secondary metabolites are present in the plant body abundantly. A peak at 900 encompasses the phosphodiester stretching band region (for absorbance due to collagen and glycogen).[35] The phosphodiester bond is a linkage between 3′ C and 5′ C atoms in deoxyribose and ribose sugar in DNA and RNA, respectively. The polysaccharide carbohydrates (glycogen) have strong binding ability with metal (Zn) and create a layer on its surface to prevent its agglomeration in the reaction medium.[36]

X-ray Diffraction (XRD) Analysis. The X-ray diffraction pattern of zinc oxide nanoparticles shows definite line broadening of the X-ray diffraction peaks, showing that the prepared particles were in the nanoscale range, as shown in Figure 1C. The diffraction peaks located at 31.5, 34.4, 36.2, 47.5, 56.4, 62.8, and 67.9° have been indexed as the spherical to the hexagonal phase of ZnO with high crystallinity[37,38] with (JPCDS card number 36-1451). It was revealed that all of the characteristic peaks were of ZnO-NPs, and no such impurities exist in synthesized ZnO-NPs. The diameter of zinc oxide crystallites was calculated by the Debye−Scherrer formula. On the bases of θ (Bragg's diffraction angle) and β (full width at half-maximum (FWHM)) of more intense peaks corresponding to 101 planes located at position 36.2°, the crystallite size is about 29 nm,[39] while the average crystallite size is 41.23 nm. The indexation confirms the standard hexagonal wurtzite structure (JCPDF file no. 00-036-1451) of ZnO-NPs, as previously reported in other studies.[40]

Thermogravimetric Analysis (TGA). The TGA spectra of ZnO-NPs indicate that the sample decomposes greatly with an increase in temperature. The sample (5 mg) was totally from 25 °C up to 600 °C loss; it was due to the different volatile components present in the sample from the plant, as shown in Figure 1D. The initial loss of the sample was due to the presence of ethanol and water in the sample. Similar weight loss was also reported by ref 41, who synthesized ZnO-NPs using aqueous extracts of *Mimosa pudica* leaves and coffee powder.

Scanning Electron Microscopy (SEM) and Transmission Electron Microscopy (TEM). The morphological study of the green synthesized zinc oxide nanoparticles was performed by SEM.[42] The particles show semispherical shape,

https://doi.org/10.1021/acsomega.1c00310
ACS Omega 2021, 6, 9709−9722

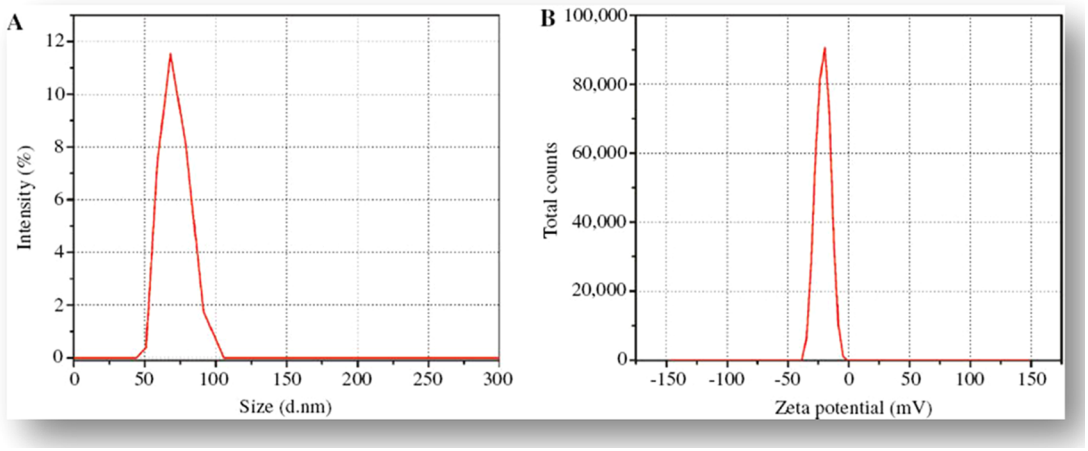

Figure 3. (A) Size distribution potential and (B) ζ-potential distribution of *M. fragrans* fruit-synthesized ZnO-NPs.

Table 1. Antibacterial Activity of *M. fragrans* Fruit-Synthesized ZnO-NPs

test organisms	activity of ZnO-NPs	antibiotics	CLSI standard	ZnO-NPs	antibiotic-coated ZnO-NPs	increase in the potency of coated ZnO-NPs
E. coli	15 ± 1.54	ciprofloxacin	21	17.3 ± 1.3	24.3 ± 1.2	32.2
		imipinem	22	19 ± 0.8	25 ± 0.87	27.3
		vancomycin	19	11 ± 1.1	14 ± 1.3	15.8
		amoxicillin−clavulanic acid	18	10 ± 1.2	14.6 ± 0.9	22.2
K. pneumoniae	27 ± 1.73	ciprofloxacin	21	16.3 ± 0.7	25.6 ± 1.4	41.4
		imipinem	22	19 ± 0.8	26 ± 1.5	31.8
		vancomycin	19	10 ± 1.1	13 ± 0.3	15.8
		amoxicillin−clavulanic acid	18	10.3 ± 0.4	14.6 ± 1.4	23.9
P. aeruginosa	17 ± 1.66	ciprofloxacin	21	15.6 ± 0.7	23 ± 1.4	35.3
		imipinem	22	20 ± 0.8	25.3 ± 1.5	24.1
		vancomycin	19	8 ± 1.1	10 ± 0.3	10.5
		amoxicillin−clavulanic acid	18	15.6 ± 0.4	18.6 ± 1.4	11.2
S. aureus	21 ± 1.73	ciprofloxacin	21	14.3 ± 0.7	26 ± 1.4	55.8
		imipinem	22	20 ± 0.8	26.6 ± 1.5	30.0
		vancomycin	19	8 ± 1.1	18.6 ± 0.3	55.7
		amoxicillin−clavulanic acid	18	10 ± 0.4	12.3 ± 1.4	12.8

and these particles are in a highly agglomerated form, as shown in Figure 2A. This clearly shows that the particles are present in a homogeneous form and the homogeneity of nanoparticles plays important roles in their different activities. The particle size ranged from 43.3 to 83.1 nm, respectively. The size increase was due to the overlapping of particles on each other. The morphology and particle size of pure zinc oxide nanoparticles were observed using TEM micrographs, as shown in Figure 2B. The presence of spherical- to hexagonal-shaped particles with a grain size of 35.5 nm was observed. We confirm the formation of ZnO-NPs by comparing the particle size obtained from X-ray diffraction and transmission electron microscopy. Our results are in harmony with previous reports.[43]

Energy-Dispersive X-ray Analysis (EDX). The EDX of the NPs reveals that there is clearly the formation of zinc oxide nanoparticles. The atomic weight of oxygen was 48.83%, while its weight present was 21%. On the other hand, the atomic weight of zinc was 37.16%, while its weight present was 65.35%, while the other minor constituents present in the ZnO-NPs were due to the presence of the root extract of ginger, as shown in Figure 2C.

ζ-Potential. The size distribution and ζ-potential of the biosynthesized ZnO-NPs were investigated using the dynamic light scattering (DLS) technique. The ζ-potential defines the colloidal stability and is a typical measurement of the surface charge on a particle. Suspensions that exhibit 15 mV are generalized as stable colloids.[44] In the study, the ζ-potential of the ZnO-NPs in distilled water (DW) was measured as −22.1 mV, and this can thus be considered as strongly anionic. The ζ-potential measurements thus verify and support the dispersion capacity of the greenly synthesized ZnO-NPs. The negative surface charge is due to the binding affinity of extract compounds with the NPs, conferring stability of the zinc oxide nanoparticles and alleviating the aggregation potential of the particles.[45] The hydrodynamic size of the particles was determined using dynamic light scattering and was found to be 66 nm for the aqueous preparation of ZnO-NPs, as shown in Figure 3A. The size distribution graph shows that the particle size is polydispersed and larger compared to that obtained from SEM observations. The increased size of the ZnO-NPs

https://doi.org/10.1021/acsomega.1c00310
ACS Omega 2021, 6, 9709−9722

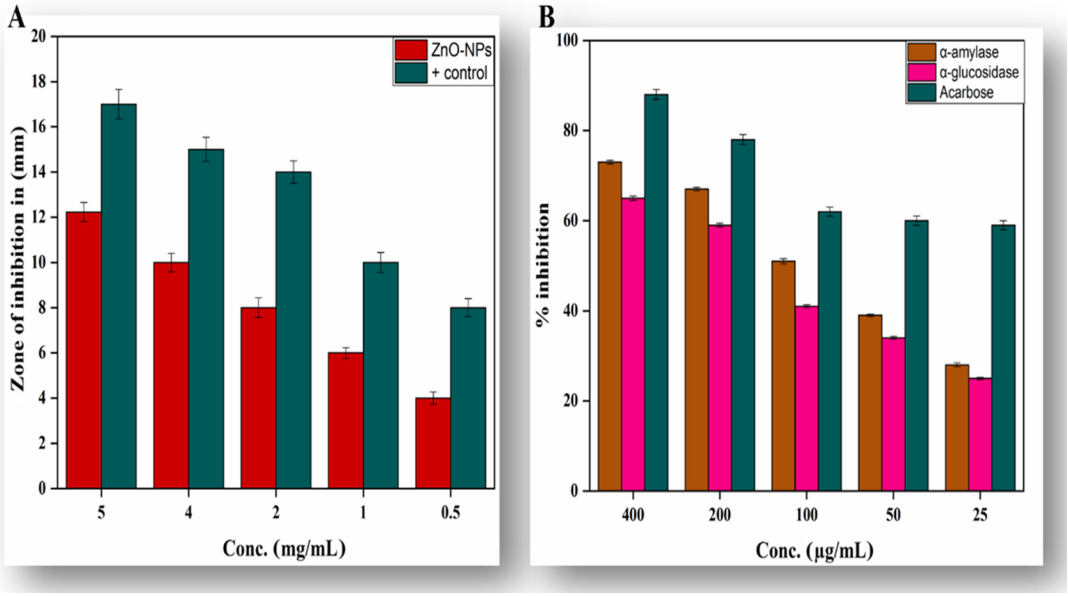

Figure 4. (A) Protien kinase inhibition and (B) antidiabetic activity of synthesized ZnO-NPs.

measured via DLS is due to the bias of the technique toward the measurement of larger particles (or even aggregates).[44] Different functional groups (carbohydrates, polysaccharides, pectin, etc.) present in plant extract adsorbed on the surface of the NPs may affect its ζ-potential. There is a close relationship between these metabolites absorbed on the surface of ZnO-NPs and ζ-potential.[46]

BIOLOGICAL APPLICATIONS

Antibacterial Assay. Antibiotic resistance is a major problem that continues to plague a broad part of the world's healthcare system of both developing and developed countries. Current antibacterial therapy has been significantly influenced by the rise and proliferation of multidrug-resistant infections. A quest for a new supply of antimicrobials such as plant-mediated nanomaterials was included, as they possess a variety of bioactive compounds with proven therapeutic properties.[47−49] In the present scenario, environmentally sustainable methods for synthesizing metallic nanoparticles have become a beneficial development. The use of plant extract phytochemicals has become a specific nanoparticle synthesis technique, as they impart a dual role of reducing and capping agents to the nanoparticles. We synthesized ZnO-NPs using a common medicinal plant in the current study and tested their antibacterial efficacy against UTI bacterial strains.[50] Table 1 depicts the complete profile of antibacterial activity of ZnO-NPs and noncoated and ZnO-NP-coated antibiotics against test organisms. In the current study, it was observed that 1% ZnO-NP solution (1 mg/mL dimethyl sulfoxide (DMSO) solution) displayed maximum zone of inhibition against *Klebsiella pneumoniae* (27 ± 1.73 mm), *Escherichia coli* (15 ± 1.54 mm), *Pseudomonas aeruginosa* (17 ± 1.66 mm), and *Staphylococcus aureus* (21 ± 1.73 mm). However, it was perceived that *E. coli*, *K. pneumoniae*, *P. aeruginosa*, and *S. aureus* displayed resistance patterns against noncoated ciprofloxacin, imipinem, vancomycin, and amoxicillin−clavulanic acid antibiotics. On the other hand, the activity of antibiotics increased significantly against these strains after being coated with ZnO-NPs. It was observed that the activity ZnO-NP-coated ciprofloxacin, imipinem, vancomycin, and amoxicillin−clavulanic acid antibiotics increased up to 32.2, 27.3, 15.8, and 22.2% against *E. coli*; up to 41.4, 31.8, 15.8, and 23.9% against *K. pneumoniae*; up to 35.3, 24.1, 10.5, and 11.2% against *P. aeruginosa*; and up to 55.8, 30, 55.7, and 12.8% against *S. aureus*, respectively. Our results are in resemblance with previous studies.[51,52]

Protein Kinase Inhibition Assay. Protein kinase enzymes play a substantial role in anticancer studies. These enzymes have the ability to phosphorylate tyrosine and serine−threonine amino acid residues that are necessary for running certain important cellular pathways like differentiation, proliferation, and cell death.[53] Uncontrolled phosphorylation caused by protein kinase enzyme produces factors that can lead to tumor growth, and entities with the potential to deter these enzymes are of significant importance in anticancer research.[54] Streptomyces 85E strain was used to elucidate the protein kinase inhibition capability of biogenic ZnO-NPs. Clear zones were observed against each tested concentration of tested ZnO-NPs. The largest bald zone of 12.23 ± 0.42 mm at 5 mg/mL and the smallest bald zone of 4.91 ± 0.17 mm were observed at 500 μg/mL. Our results are in accordance with the literature available on ZnO-NP kinase inhibition enzymes.[55] Overall results concluded that the biogenic NPs acquire vital capping and stabilizing agents from plant extracts responsible for anticancerous capability. Biogenic ZnO-NPs were observed to inhibit Streptomyces strain in a dose-dependent manner, as shown in Figure 4A.

Antidiabetic Activity. Diabetes mellitus (DM) is a metabolic condition characterized by chronic hyperglycemia due to reduced insulin production or insensitivity of body cells to insulin that has already been produced.[56] There were 425 million people living with DM, according to the International Diabetes Federation (IDF) survey for 2017, and this number will increase to 629 million by 2045.[57] One effective clinical strategy for the treatment of DM is the reduction of postprandial hyperglycemia, which can be done by inhibiting α amylase and α glucosidase, the two most important carbohydrate hydrolyzing enzymes in the digestive tract.[56] A

https://doi.org/10.1021/acsomega.1c00310
ACS Omega 2021, 6, 9709−9722

Table 2. Antioxidizing Potential of Synthesized ZnO-NPs

conc (μg/mL)	TAC (μg AAE/mg)	TRP (μg AAE/mg)	ABTS (TEAC)	DPPH (%FRSA)
400	71.1 ± 0.83	63.41 ± 0.83	82.12 ± 0.28	66.3 ± 0.28
200	62.37 ± 0.27	57.51 ± 0.87	74.63 ± 0.39	51.1 ± 0.71
100	54.86 ± 0.72	43.23 ± 0.26	67.64 ± 0.56	37.69 ± 0.32
50	35.29 ± 0.76	27.76 ± 0.58	55.47 ± 0.26	28.45 ± 0.98
25	29.16 ± 0.25	17.41 ± 0.36	40.39 ±0.15	20.19 ± 0.48

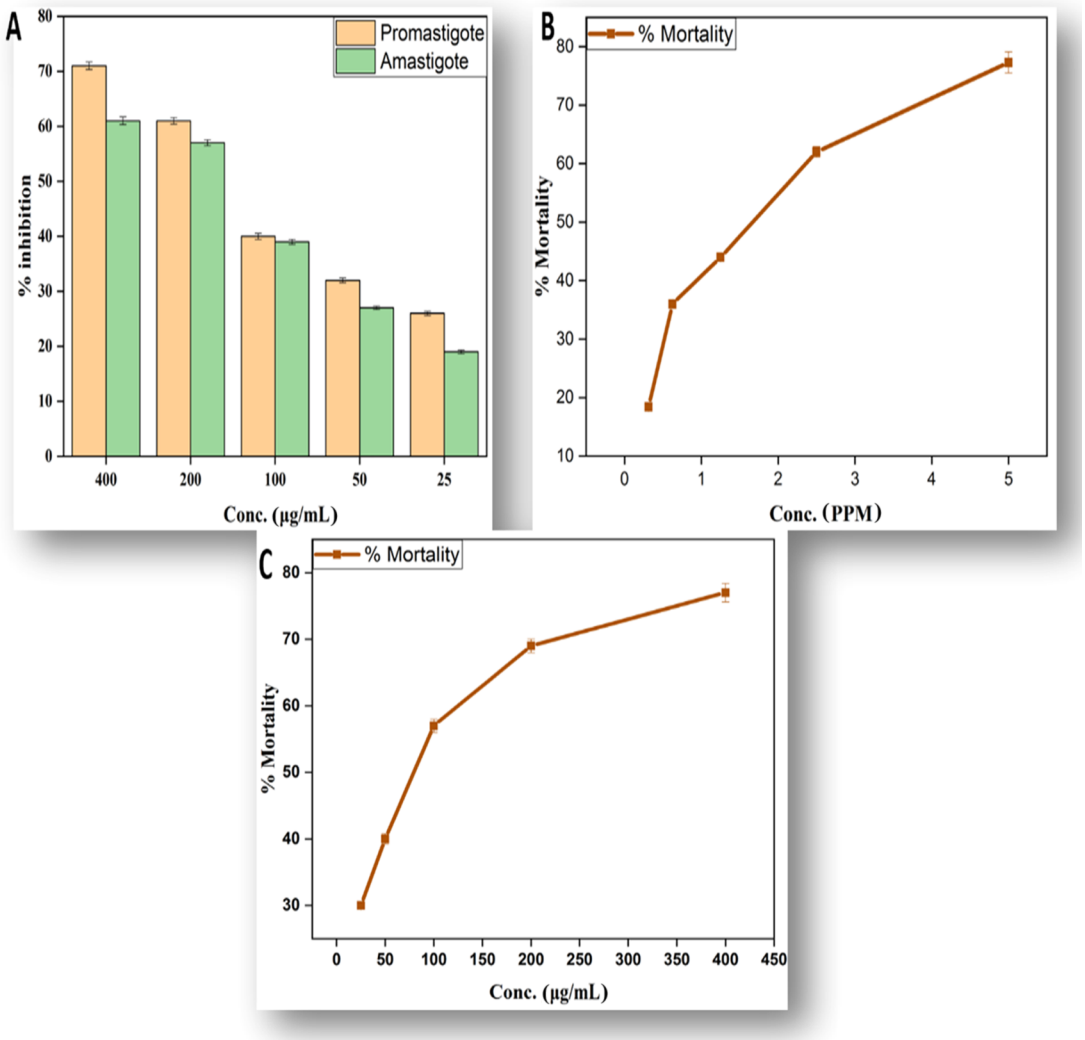

Figure 5. (A) %Mortality of amastigote and promastigote, (B) antilarvicidal activity, and (C) brine shrimps' lethality assay of ZnO-NPs.

point of enormous importance is the search for new sources of natural products with probable antidiabetic action from tropical flora and nanotools. In this study, nanoparticle samples of zinc oxide NPs were evaluated for α-amylase and α-glucosidase inhibition, as shown in Figure 4B. Our findings indicated excellent α-amylase and α-glucosidase inhibition activity. Maximum inhibition of about 73.23 ± 0.42 for α-amylase and 65.21 ± 0.49 for α-glucosidase was calculated at 400 μg/mL. Our results are in agreement with a previous report conducted on several classes on NPs.[58,59] Here, we show that biobased nanoparticles can exhibit tremendous antidiabetic behavior and are considered to be an effective therapeutic agent for the treatment of diabetes as an alternative to the use of costly and less efficient drugs.

Antioxidant Assay. The change in plant metabolic pathways is attributed to environmental stress that results in reactive oxygen species (ROS) destroying membrane lipids, plant cells, DNA, and proteins.[60] Many metabolically important compounds like flavonoids, terpenoids, and oxidative stress-responsive agents play a promising role in the capping and stabilization of the nanoparticles.[61,62] Four separate assays, i.e., total antioxidant capacity (TAC), total reduction power (TRP), 2,2′-azino-bis(3-ethylbenzothiazoline-6-sulfonic acid) (ABTS), and 2,2-diphenyl-1-picrylhydrazyl (DPPH) free radical scavenging assay (FRSA), were conducted to assess the *in vitro* antioxidant potential of plant-synthesized NPs. We summarize the phosphomolbdenum-based technique to find the dose-dependent antioxidant potential of biogenic ZnO-NPs. This technique is based on the

https://doi.org/10.1021/acsomega.1c00310
ACS Omega 2021, 6, 9709−9722

reduction of Mo(VI) to Mo(V) with the help of an antioxidant mediator that results in the formation of phosphate-molybdate, and the color of phosphate-molybdate is green, which helps in its identification.[63,64] Antioxidant capacity of biogenic ZnO-NPs in comparison to that of ascorbic acid is recorded to be 71.1 ± 0.83 μg AAE/mg at 400 μg/mL. Total antioxidant capacity (TAC) was amplified with the total reducing power estimation (TRP) assay. If the tested sample possesses redox potential, it will convert the Fe^{+3} to Fe^{+2} ion.[65] Like TAC, the highest TRP was noted as 63.41 ± 0.83 at the highest tested concentration. Furthermore, to support the TAC and TRP findings, ABTS (2,2′-azino-bis(3-ethylbenzothiazoline-6-sulfonic acid)) and DPPH (2,2-diphenyl-1-picrylhydrazyl) free radical scavenging assays were also performed. DPPH is a stable free radical that is reduced by accepting hydrogen or electron from a donor based on formation of a yellowish diphenyl picrylhydrazine molecule.[66] These spectrophotometric methods are based on quenching of stable colored radicals of DPPH and ABTS, indicating the scavenging ability of the antioxidant sample. In the study, excellent free radical scavenging activity of all test concentrations was revealed, as summarized in Table 2. The highest DPPH and ABTS free radical scavenging activities at 400 μg/mL were noted as 66.3 ± 0.28 and 82.12 ± 0.28 TEAC for ZnO-NPs, respectively. All of these assays were carried out in triplicates, and the values were recorded as means of their triplicates. Our results are in harmony with previous reports.[50,67]

Antileishmanial Assay. Leishmaniasis is a severe, non-contagious, infectious disease caused mainly by parasites present in the genus Leishmania. Leishmaniasis is one of the six major infectious diseases in tropical and subtropical countries, with a mortality rate of 50 000 deaths per year, according to the World Health Organization (WHO).[68] The disease is at high risk of unregulated dissemination due to inadequate vectors and inefficient and inexpensive medicines. Metal oxide nanoparticle (zinc, silver, titanium, and magnesium oxide)-related therapies have recently become common due to their strong cytotoxic ability toward Leishmania.[69] We use different concentrations of the biogenic ZnO-NPs from 25 to 400 μg/mL for finding out their antileishmanial activity against amastigotes and promastigotes using the 3-(4,5-dimethylthiazol-2-yl)-2,5-diphenyltetrazolium bromide (MTT) assay, as illustrated in Figure 5A. At the highest concentration of 400 μg/mL, the biogenic NPs possess the potent mortality rate of 71.50 ± 0.70 for promastigotes and 61.41 ± 0.71 for amastigotes. The lowest mortality rate recorded for biogenic ZnO-NPs was 26.90 ± 0.39 for promastigote and 19.60 ± 0.33 for amastigote. The results of our study are in agreement with previous studies.[28,70]

Antilarvicidal Activity. In recent decades, the prevalence of dengue has risen significantly around the world. About 2.5 billion people, two-fifths of the world's population, are already at risk from dengue. The WHO currently predicts that there could be 50 million dengue infections worldwide per year.[71] *Aedes aegypti* L., a dengue vector carrying the liable arbovirus, is commonly spread in the tropical and subtropical areas in recent times. Fighting the disease-carrying mosquitoes is the best way to avoid the dengue virus spread.[72] Material scientists in recent times are more focused to find better alternatives using plant extracts and plant-mediated NPs against the propsed vector. In the present study, a range of concentrations of synthesized NPs (0.3125, 0.6250, 1.25, 2.5, 5 ppm) were tested against the second and fourth instars of *A. aegypti*. In total, 77.3 ± 1.8% mortality was observed at 5 ppm followed by 18.4 ± 0.44% at 0.3125 ppm, as shown in Figure 5B. At subsequently reduced concentrations, mortality reduced in parallel.

Brine Shrimp Lethality Assay. In recent years, the role of brine shrimp in aquaculture has become important. In winter, about 10 million pounds of brine shrimp eggs are harvested and marketed as food for tropical fish.[73] Artemia is an appropriate organism for research of bioassays and toxicity. In the aquatic food chain, this species has a central function.[74] The main aim of our study is to find the acute toxicities of ZnO-NPs. Concentrations are applied in a higher dose manner from 25 to 400 μg/mL. The highest mortality value of 77 ± 1.4 is observed at 400 μg/mL. The toxicity pattern of metallic NPs toward *Artemia salina* is dose-dependent. The lowest value of 30 ± 0.44 is observed at 25 μg/mL, as shown in Figure 5C. The results of NPs themselves, dissolution products, and agglomerates of NPs formed during the experiment can result in toxicity of NPs. The findings of this analysis showed that proper consideration should be paid to the possible eco-toxicity and environmental health consequences of NPs.[75,76]

***In Vitro* Biocompatibility Studies.** For the demonstration of the biocompatibility of the green synthesized NPs, a biocompatibility assay was performed using human red blood cells. In this bioassay, hemolysis of the human red blood cells is noted against various concentrations of the nanoparticles (25−400 μg/mL). Hemolysis of RBCs is measured at 405 nm using a spectrophotometer. The hemolysis of RBCs will only be observed if the sample has the ability to rupture the cells. The biocompatibility results of our study are listed in Table 3. The

Table 3. % Hemolysis of Green Synthesized ZnO-NPs

Sl no.	conc. (μg/mL)	% hemolysis
1	400	3.58 ± 0.11
2	200	2.46 ± 0.14
3	100	0.97 ± 0.09
4	50	0.53 ± 0.06

American Society for Testing Materials has issued some guidelines for biocompatibility of substances, and according to that guidelines, substances having >2% hemolysis are labeled as nonhemolytic, 2−5% slightly hemolytic, and >5% are considered as hemolytic.[77] As can be seen from Table 3, all our stock solutions of synthesized nanoparticles show less hemolysis even at high concentrations, which shows their high biocompatibility. To use NPs for biomedical applications, we have to check their biocompatibility. Synthesised biogenic ZnO-NPs are hem-compatible, and even at a high concentration of 400 μg/mL, we observed no hemolytic activity. The biocompatibility results of our study thus show that plant-based synthesized nanoparticles are biosafe and we can use ZnO-NPs for therapeutic purposes.

PHOTOCATALYTIC ACTIVITIES OF ZN-NPS FOR THE DEGRADATION OF METHYLENE BLUE DYE

Effect of Irradiation Time. With an increase of UV light illumination in the initial 20 min, the degradation was observed at 19.6%, while with a further increase in time, the degradation of dye also increased and the maximum degradation was observed at 140 min, which was 88%, as shown in Figure 6a,b.

Mechanism of Photocatalytic Catalytic Degradation of the Dye. We have already studied the relationship between

https://doi.org/10.1021/acsomega.1c00310
ACS Omega 2021, 6, 9709−9722

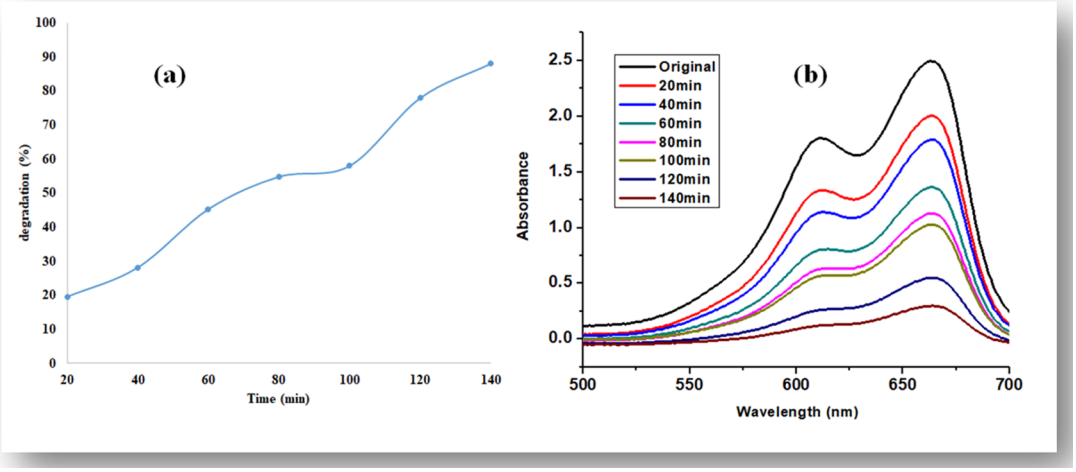

Figure 6. (a) Percent degradation of methylene blue dye with ZnO nanoparticles and (b) UV−visible spectra.

the time and the degradation process; now, we need to know how this degradation process happens. The effect of time on the degradation process was studied to know the mechanism.[78] The light-dependent degradation process of methylene blue dye is illustrated in Scheme 1. First, the dye is adsorbed on the surface of the catalyst (zinc in this case) and then it is exposed to ultraviolet light illumination to excite valence electrons so the electrons may transfer to the conduction band from the valence band; during the process, a positive hole h^+ is lifted inside the valence band. The positive holes and free electrons will react on the surface of the photocatalyst along with adsorbed water molecules, and as a result, the positive holes will react with water to produce $^{\bullet}OH^-$ radicals and the free electrons reduce the dissolved oxygen to superoxide anion $O_2^{\bullet-}$ radicals. These light-generated radicals degrade the dye molecules into simple molecules such as CO_2 and H_2O.[79]

Scheme 1. Reaction Mechanism for the Degradation of Methylene Blue

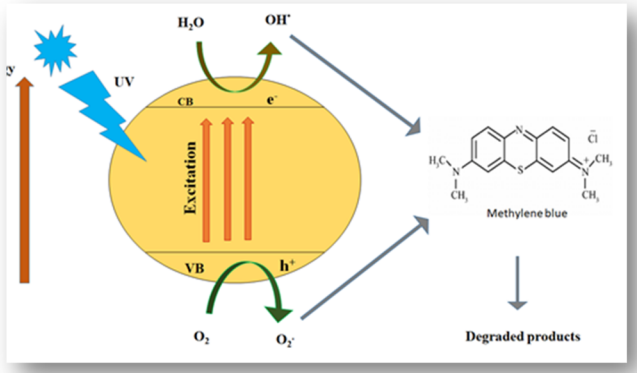

$$ZnO + h\nu \rightarrow e^- + h^+ \quad (1)$$

$$H_2O + h^+ \rightarrow {}^{\cdot}OH{\cdot} + H^+ \quad (2)$$

$$O_2 + e^- \rightarrow {}^{\cdot}O_2{\cdot}- \quad (3)$$

$$^{\cdot}OH + \text{dye} \rightarrow \text{degradable product} \quad (4)$$

$$O_2^- + \text{dye} \rightarrow \text{degradable product} \quad (5)$$

CONCLUSIONS

This research work is basically focused on one-pot eco-friendly plant-based synthesis of biomedically important ZnO-NPs using aqueous fruit extracts of *M. fragrans*, a medicinally important plant. XRD analysis has verified the crystalline structure of the synthesized NPs. Fourier transform infrared (FTIR) spectroscopy analysis verified the existence of phytochemicals involved in the transfer of metallic ions to NPs. Morphologies and vibrational modes were determined by SEM and TEM analyses, DLS determined the surface charge and stability, and also the stability is determined by TGA. Synthesized ZnO-NPs have shown successful capacity for antioxidants and against bacterial strains. There is moderate inhibitory ability for bioengineered ZnO-NPs against α-amylase and α-glucosidase enzymes. Biogenic ZnO-NPs were found to have significant potency against brine shrimps and larvae of *A. aegypti*. The synthesized ZnO-NPs were also effective in the degradation of methylene blue dye. Synthesized ZnO-NPs were also documented to be biocompatible with human red blood cells. Our research work concluded that the above-mentioned biogenic ZnO-NPs can be used for different studies in diseases, cosmetics, and cancers. More research on zinc oxide nanoparticles is needed to explore their applications in biomedicine at both *in vitro* and *in vivo* levels.

METHODS

Plant Collection and Extraction. *M. fragrans* fruits were purchased from a local market in Pakistan. The plant material was converted into fine powder through an electric grinder for the preparation of extracts. The plant powder (50 g) was soaked in 500 mL of distilled water and heated at 150 °C for 20 min. For maximum extraction, the soaked powder was kept in an incubator at 37 °C overnight. The extract was filtered through Whatman filter paper no. 1823, and then, the solvent was evaporated through a rotatory evaporator at 40 °C. The obtained extract was preserved in a refrigerator at 4 °C.

Synthesis of ZnO-NPs. Zinc oxide nanoparticles were synthesized according to a previously described protocol with slight modifications. Briefly, 6.0 g of zinc acetate dihydrate ($Zn(NO_3)_2{\cdot}2H_2O$) (Sigma-Aldrich) was added to 100 mL of extract and kept on a magnetic stirrer at 60 °C for 2 h. Once the reaction was complete, the mixture was allowed to cool down at 25 °C and centrifuged (HERMLE Z326K) at 10 000

https://doi.org/10.1021/acsomega.1c00310
ACS Omega 2021, 6, 9709−9722

rpm for 10 min. The supernatant was discarded, and the remaining pellet was washed thrice with distilled water, poured into a clean Petri plate, and oven-dried at 90 °C. The dried material was then ground into fine powder in a pestle and mortar and calcined for 2 h at 500 °C to remove any impurities. The annealed powder was stored in an airtight glass vial, labeled as ZnO-NPs, and was further used for physical characterizations and biological applications.[28]

Characterization of Biosynthesized ZnO-NPs. To analyze the physiochemical properties of ZnO-NPs, different characterization techniques have been used to analyze the physicochemical properties of ZnO-NPs synthesized from *M. fragrans*. These techniques include UV spectroscopy, Fourier transform infrared (FTIR) spectroscopy, X-ray diffraction (XRD), scanning electron microscopy (SEM), transmission electron microscopy (TEM), energy-dispersive X-ray (EDX) analysis, dynamic light scattering (DLS), and thermogravimetric analysis (TGA).

The reaction carried out between the extract and zinc nitrate solution was analyzed using UV−visible spectroscopy in the range of 200−700 nm. To detect the nature of green synthesized zinc oxide nanoparticles, the X-ray diffraction technique was used. A PANalytica X'pert X-ray diffractometer was used to obtain the X-ray diffraction pattern. For finding the size of the crystallite, we use Scherer's equation[80]

$$D = k\lambda/\beta \cos\theta$$

where D represents the half peak height of an XRD line due to a specific crystalline plane, k denotes the shape factor (0.94), λ depicts the X-ray wavelength of 1.5421 Å, and β and θ refer to FWHM in radian and Bragg's angle, respectively. The functional group responsible for the formulation of nanoparticles was detected using Fourier transform infrared (FTIR) spectroscopy in the spectral range of 400 and 4000 cm^{-1}. Morphologies and physical dimensions were examined by SEM (JSM-7600F, Japan) and TEM (JEM-2100F, Japan), while elemental analysis was conducted using energy-dispersive X-ray spectroscopy (EDX).[81]

The electrostatic potential that occurs at the shear plane of a particle, which is of concern to both the surface charge and the local medium of the particle is known as ζ-potential. We analyze the ζ-potential using a zeta potential analyzer. We use phase analysis light scattering mode and maintain proper room temperature for recording all of the measurements. For the calculation of the ζ-potential, we use the Smoluchowski equation mentioned below.

$$v = (\varepsilon E/\eta)\xi$$

where v = electrophoretic velocity, η = viscosity, ε = electrical permittivity of the electrolytic solution, and E = electric field.[82]

Thermogravimetric analysis was carried out using a Q500 thermogravimetric analyzer for the investigation of thermal stability. For the above purpose, 5 mg of the tested sample was decomposed under flowing nitrogen gas from 30 to 600 °C at 10 °C/min heating rate.

BIOLOGICAL APPLICATIONS

Antibacterial Activities. *Bacterial Species Collection.* Overall, four MDR strains *K. pneumoniae*, *E. coli*, *P. aeruginosa*, and *S. aureus* were analyzed for confirmation of antibacterial activity. The strains were already isolated from patients with urinary tract infections. All of these isolates were collected from Hayat Abad Medical Complex Peshawar (HMC), Pakistan. Biochemical and molecular tests (16s RNA) were done at the hospital for the identification of these UTI isolates.

ZnO-NP-Coated Antibiotic Disc Preparation. Zinc oxide nanoparticle residues (20 mg) were mixed with 1 mL of distilled water to prepare the stock solution of powdered ZnO-NPs. After complete mixing, we take 5 μL from the prepared stock solution, poured it on the antibiotic disc, and placed the disc inside the oven for drying at 80 °C and for 15 min. The same procedure was used for each antibiotic.

Agar Well Diffusion Assay for ZnO-NPs. The wells, having 8 mm diameter, were punched into the nutrient agar (NA) media followed by bacterial lawn preparation in the media.[83] The wells were filled with 100 μL of ZnO-NP suspension. The Petri dishes were then kept in an incubator at 37 °C for 24 h. Just after the incubation, the potency of ZnO-NPs against the tested MDR bacterial strains was determined by measuring zones of inhibition in millimeters.

Disc Diffusion Assay for Antibiotic Discs and Antibiotic-Coated ZnO-NPs. To evaluate the potency of both coated and noncoated antibiotics against tested MDR bacterial strains, the standard Kirby Bauer disc method was used. Nutrient agar was prepared, and then, NA media along with Petri dishes were autoclaved using standard SOPs. After the medium was sterilized, it was cooled to 50 °C and then poured into sterilized Petri dishes in a biosafety cabinet. After the media were solidified, bacterial lawns were prepared on nutrient agar (NA) plates, then both ZnO-NP-coated and noncoated antibiotic discs were applied, and the Petri plates were incubated at 37 °C for 24 h. After incubation, the potency of both coated and noncoated antibiotics against test MDR bacterial strains was determined by measuring zones of inhibition in millimeters.

Protein Kinase Inhibition Assay. For screening the anticancer activity of biosynthesized ZnO-NPs, a protein kinase inhibition assay was performed. This is a preliminary bioassay for the confirmation of the protein kinase inhibitory ability of the synthesized NPs. Our protocol was slightly different from that followed by ref 28. A test strain of Streptomyces 85E was used. We prepare the plate containing sterile ISP4 medium and then transferred a volume of 100 μL from the refreshed culture of Streptomyces 85E to the plates. About 5 μL of ZnO-NPs was poured inside each well (5 mm) and labeled accordingly. Surfactin and DMSO worked as positive and negative controls. After this, all of the plates were subjected to incubation at 28 °C for 2 days. We observed clear and bald zones around wells, indicating the inhibition of phosphorylation, mycelia, and formation of spores. A Vernier calliper was used for the measurement of the zones to the nearest millimeter. The clear zones show the cytotoxic potential of ZnO-NPs and death of the test strain.

Antidiabetic Assay. The antidiabetic activity of the biogenic ZnO-NPs was determined using α-glucosidase and α-amylase inhibition assays.

α-Amylase Inhibition Assay. For the evaluation of the α-amylase inhibition assay of the biogenic ZnO-NPs, we used the most acceptable protocol with some minor changes.[84] To perform this assay, we used a 96-well microplate. Inside each well, we poured phosphate buffer (15 μL), α-amylase (25 μL), sample (10 μL), and starch (40 μL). After this, the plate was subjected to incubation at 50 °C for 30 min. At last, 20 μL of HCl solution and 90 μL of iodine were added to each well. For negative control, we used DMSO, and for positive control, acarbose was used, while the blank contained buffer solution

https://doi.org/10.1021/acsomega.1c00310
ACS Omega 2021, 6, 9709−9722

and starch instead of ZnO-NPs. A microplate photometer was operated at 540 nm for the observing the sample absorbance capacity. We calculated the percentage inhibition with the following formula.

$$\%\ \text{enzyme inhibition} = \left(\frac{\text{Abs sample} - \text{Abs negative control}}{\text{Abs blank} - \text{Abs negative control}}\right) \times 100$$

α-Glucosidase Inhibition Assay. ZnO-NPs' antidiabetic activity was demonstrated using the α-glucosidase inhibition assay.[85] For dissolving α-glucosidase (*Saccharomyces cerevisiae*, Sigma-Aldrich), 50 mL of phosphate buffer having pH 6.8 was supplemented with 100 mg of bovine serum albumin. The reaction mixture prepared using 10 μL of tested sample, phosphate buffer (490 μL; pH 6.8), and *p*-nitrophenyl α-D-glucopyranoside (5 mM; 250 μL) was kept in an incubator at 37 °C for 5 min. α-Glucosidase (0.15 units/mL; 250 μL) was then introduced to samples followed by reincubation for 15 min at 37 °C. After terminating the reaction by adding 2 mL of Na_2CO_3 (200 mM) solution, absorption spectra were recorded using a UV−vis spectrophotometer at 400 nm. The assay is based on the quantification of *p*-nitrophenol released from *p*-nitrophenyl α-D-glucopyranoside. In the experiment, acarbose was employed as the positive control, and the experiment was repeated thrice.

$$\%\text{enzyme inhibition} = \left(\frac{\text{Abs sample} - \text{Abs negative control}}{\text{Abs blank} - \text{Abs negative control}}\right) \times 100$$

Antioxidant Assays. *Total Antioxidant Capacity Determination (TAC).* For examination of total antioxidant capacity, the same assay was used as reported by ref 86. Eppendorf tubes were filled with 100 μL of sample using a micropipette. Then, we added 900 mL of TAC reagent to Eppendorf tubes (0.6 M sulfuric acid, 28 mM sodium phosphate, and 4 mM ammonium molybdate, in 50 mL of dH_2O). The reaction mixture was then incubated at 90 °C for 2 h in a water bath; after cooling the samples, absorbance was recorded at 630 nm by a microplate reader. The above-mentioned procedure was performed three times; TAC was expressed as μg ascorbic acid equivalent/mg of sample.

Total Reducing Power (TRP) Determination. For finding out the total reducing power (TRP), the same procedure was followed as reported by ref 87. The Eppendorf tube already containing 100 μL of the test sample was filled with 400 μL of 0.2 M phosphate buffer having pH 6.6 and potassium ferric cyanide (1% w/v); after this, the tube containing all of these samples was incubated in a water bath for 30 min at 55 °C. After incubation, 400 μL of trichloroacetic acid (10% w/v) was added to each Eppendorf tube and the Eppendorf tube was subjected to centrifugation for 10 min at a speed of 3000 rpm. After centrifugation, the supernatant (140 μL) obtained was poured into wells of a 96-well plate, which already contained 60 μL of ferric cyanide solution (0.1% w/v); using a microplate reader at 630 nm, we then recorded the absorbance of the sample. The procedure mentioned above was used for both positive and negative controls.

Free Radical Scavenging Assay (FRSA). For finding the free radical scavenging ability of the biosynthesized and eco-friendly zinc oxide nanoparticles, we follow the same protocol used by ref 84 with some modifications. ZnO-NPs' free radical scavenging is their antioxidant potential and was investigated using the DPPH reagent. The activity was recorded at both the lowest (12.5 μL) and highest (400 μL) concentrations. First, we poured the tested sample of concentration (10 μL) inside the wells of a 96-well plate and then added (190 μL) DPPH reagent to every well already containing the tested samples. After this, the samples were subjected to incubation in the dark at a temperature of 37 °C for 60 min. For FRSA, we used both a positive control (ascorbic acid) and a negative control (DMSO). For recording the absorbance rate of the sample, we used a microplate photometer at 515 nm. Free radical scavenging ability of the biogenic ZnO-NPs was determing using the following equation

$$\%\text{FRSA} = \left(1 - \frac{\text{Abs}}{\text{Abc}}\right) \times 100$$

Abc and Abs indicates the absorbances of the negative control and sample, respectively.

Trolox Antioxidant Assay (ABTS). The ABTS assay was used for finding the antioxidant activity of the biogenic ZnO-NPs. First, we mixed potassium persulfate (2.45 mM) and 7 mM ABTS salt in equal concentrations and then incubated the mixture at room temperature. After incubating the samples at room temperature, the mixture prepared above from potassium persulfate and ABTS salt were kept in the dark for 15 min. The sample absorbance was recorded using a BioTek ELX800 at 734 nm. To perform the assay, we take both positive (Trolox reagent) and negative (DMSO) controls. The process was repeated three times, and antioxidant results were expressed as TEAC.

Antileishmanial Assay. Biogenic ZnO-NPs were evaluated for their antileishmanial activity against both amastigotes and promastigotes using the standard protocol described previously.[88] *Leishmania tropica* KWH23 strain was used for evaluating anti-leshminial activity of the biogenic zinc oxide nanoparticles; for this purpose, we incubated the culture of *L. tropica* KWH23 strain in MI99 medium, which was already supplemented with fetal bovine serum (FBS). First, we took 20 μLof tested sample and poured it in a 96-well plate and then we added 180 μL of aliquot into the wells of the 96-well plate; the aliquot was taken from the suspension culture (seeding density 1×10^6 cells/mL). After this, we incubated the mixture at room temperature (25 °C) for 72 h. We took Amphotericin B as the positive control and DMSO (1%) in phosphate-buffered saline (PBS) as the negative control. After the incubation, we poured 20 μL of MTT solution (4 mg/mL in dH_2O) inside each well and again incubated the culture plate for 4 h at room temperature (25 °C). A microplate reader was used to record the absorbance of the samples at 540 nm. The percent inhibition was calculated using the formula

$$\%\text{inhibition} = \left[1 - \left\{\frac{\text{absorbance of sample}}{\text{absorbance of control}}\right\}\right] \times 100$$

The sample was analyzed again using different concentrations, and the process was repeated three times. The IC_{50} values were revealed using TableCurve 2D software v5. 01.

Larvicidal Assay. For finding out the larvicidal potential of biogenic ZnO-NPs, the same protocol was used as proposed by the World Health Organization.[36] For this assay, four experimental groups and one control group were designed. A

https://doi.org/10.1021/acsomega.1c00310
ACS Omega 2021, 6, 9709−9722

plastic well containing 25 third instar larvae and 200 mL of tested suspension was used for the experimental group, while the same was done in distilled water for the control group. Four technical replicates were designed for each group containing 500 larvae per larvicidal assay simplified as (100 larvae per concentration × 4 concentrations) + (100 larvae per control group). This assay was done three times.. We provided standard insectary condition "28 ± 1 °C temperature, 80 ± 10% relative humidity, and 12 h light/12 h darkness photoperiod"; the purpose of the condition was to maintain larvae while performing the bioassay. We provided no food for 24 h after beginning the bioassay; the purpose was to record the mortality rate of the larvae during the bioassay. The mortality was detected by the common technique by providing stimulus to the larvae; if they did not respond or move slightly but not vigorously, they were considered dead.[89]

Brine Shrimp Cytotoxicity. This activity was accomplished to determine the cytotoxic effectiveness of ZnO-NPs.[90] Purchased eggs of *A. salina* from Ocean Star International were stocked at 28 °C. The eggs were allowed to hatch in 34 g/L artificial seawater in a tray near a light source at 37 °C. Ten fresh hatched nauplii were taken and transferred to each well. Test samples (12.5−200 μg/mL) were poured into each well, and the adjusted volume was 300 μL at this stage. The shrimps were observed and counted under a magnifying lens, after a complete 24 h of exposure. The TableCurve tool was used to determine LD; the percentage was also determined for dead shrimps using mathematical formulas. For observing the brine shrimp, we used the following concentrations of biogenic ZnO-NPs in ppm: 0.2, 0.3, 0.4, 0.5.

Biocompatibility Study. Biogenic ZnO-NPs' biocompatibility was demonstrated using fresh human red blood cells (hRBCs).[91] Blood samples (1 mL) were taken from healthy individuals in ethylenediaminetetraacetic acid (EDTA) tubes after permission of the individual. After collection of blood samples, the samples were subjected to centrifugation for the isolation of RBCs. After centrifugation, supernatant and pellet were obtained; the supernatant was discarded, and the pellet was collected after washing three times with PBS. For the preparation of PBS−erythrocyte suspension, we mix 200 μL of RBCs with 9.8 mL of PBS (pH 7.2). Then, the suspensions of erythrocytes and green synthesized ZnO-NPs were mixed in Eppendorf tubes. The Eppendorf tubes containing the mixture of erythrocyte suspension and biogenic NPs were then subjected to incubation for 1 h at 35 °C. Reaction mixtures were centrifuged at 1000 rpm for 10 min followed by transfer of 200 μL of supernatant to a 96-well plate; and hemoglobin release absorption spectra were recorded at 540 nm. As a control, Triton X-100 (0.5%) was used, while DMSO was considered as a negative control. %hemolysis was calculated using the following formula

$$\%\text{hemolysis} = \left(\frac{\text{sample Ab} - \text{negative control Ab}}{\text{positive control Ab} - \text{negative control Ab}}\right) \times 100$$

where Ab stands for the absorbance of the samples as recorded.

Photocatalytic Activity. To find out the photocatalytic activity of the biogenic zinc oxide nanoparticles, we prepared 20 ppm of methylene blue dye in 50 mL of deionized water.[92] The original concentration (5 mL) was taken from the solution, while the remaining solution of 25 mg (0.025 g) of ZnO-NP catalyst was added to 45 mL of dye solution; for maintaining the adsorption−desorption equilibrium, the solution was placed in the dark for 20 min, then the solution was subject to UV light, and the sample was taken after every 20 min. Centrifugation was performed at 10 000 rpm for 15 min to remove the catalyst from the samples; the degradation of dye was studied by a UV−visible spectrophotometer. The percent degradation of the degraded dye was calculated by the following formula

$$\% = \frac{C_0 - C_t}{C_0} \times 100$$

$$\% = \frac{A_0 - A_t}{A_0} \times 100$$

where C_0 and A_0 are the initial concentrations of the dye and C_t and A_t are the concentrations after a time interval.

AUTHOR INFORMATION

Corresponding Author

Shah Faisal − *Department of Biotechnology, Bacha Khan University, Charsadda 24460, KPK, Pakistan;* orcid.org/0000-0001-5474-2622; Email: shahfaisal11495@gmail.com

Authors

Hasnain Jan − *Department of Biotechnology, Bacha Khan University, Charsadda 24460, KPK, Pakistan; Department of Biotechnology, Quaid-i-Azam University, Islamabad 45320, Pakistan*

Sajjad Ali Shah − *Department of Biotechnology, Bacha Khan University, Charsadda 24460, KPK, Pakistan*

Sumaira Shah − *Department of Botany, Bacha Khan University, Charsadda 24460, KPK, Pakistan*

Adnan Khan − *Institute of Chemical Sciences, University of Peshawar, Peshawar 25120, KPK, Pakistan*

Muhammad Taj Akbar − *Department of Microbiology, Abdul Wali Khan University, Mardan 23200, KPK, Pakistan*

Muhammad Rizwan − *Center for Biotechnology and Microbiology, University of Swat, Mingora 19130, KPK, Pakistan*

Faheem Jan − *Programmatic Management of Drug Resistant T.B. Unit, Ayub Teaching Hospital, Abbotabad 22040, Pakistan*

Wajidullah − *Department of Chemistry, Bacha Khan University, Charsadda 24460, KPK, Pakistan*

Noreen Akhtar − *Department of Microbiology, Khyber Medical University, Peshawar 25100, KPK, Pakistan*

Aishma Khattak − *Department of Bioinformatics, Shaheed Benazir Bhutto University, Peshawar, KPK, Pakistan*

Suliman Syed − *Department of Biotechnology, Bacha Khan University, Charsadda 24460, KPK, Pakistan*

Complete contact information is available at: https://pubs.acs.org/10.1021/acsomega.1c00310

Notes

The authors declare no competing financial interest.

ACKNOWLEDGMENTS

The authors are grateful to the Department of Biotechnology, Bacha Khan University, Pakistan for providing research facilities.

https://doi.org/10.1021/acsomega.1c00310
ACS Omega 2021, 6, 9709−9722

REFERENCES

(1) Ramsden, J. *Nanotechnology: An Introduction*; William Andrew, 2016.
(2) Albrecht, M. A.; Evans, C. W.; Raston, C. L. Green chemistry and the health implications of nanoparticles. *Green Chem.* **2006**, *8*, 417−432.
(3) Herlekar, M.; Barve, S.; Kumar, R. Plant-mediated green synthesis of iron nanoparticles. *J. Nanopart.* **2014**, *2014*, No. 140614.
(4) Simonis, F.; Schilthuizen, S. *Nanotechnology; Innovation Opportunities for Tomorrow's Defence*; TNO Science & Industry Future Technology Center: The Netherlands, 2006.
(5) Iravani, S. Green synthesis of metal nanoparticles using plants. *Green Chem.* **2011**, *13*, 2638−2650.
(6) Duan, H.; Wang, D.; Li, Y. Green chemistry for nanoparticle synthesis. *Chem. Soc. Rev.* **2015**, *44*, 5778−5792.
(7) Bala, N.; Saha, S.; Chakraborty, M.; Maiti, M.; Das, S.; Basu, R.; Nandy, P. Green synthesis of zinc oxide nanoparticles using Hibiscus subdariffa leaf extract: effect of temperature on synthesis, antibacterial activity and anti-diabetic activity. *RSC Adv.* **2015**, *5*, 4993−5003.
(8) Hasan, S. A review on nanoparticles: their synthesis and types. *Res. J. Recent Sci* **2015**, *4*, 1−3.
(9) Barzinjy, A. A.; Hamad, S. M.; Aydın, S.; Ahmed, M. H.; Hussain, F. H. Green and eco-friendly synthesis of Nickel oxide nanoparticles and its photocatalytic activity for methyl orange degradation. *J. Mater. Sci.: Mater. Electron.* **2020**, *31*, 11303−11316.
(10) Altavilla, C.; Ciliberto, E. In *Inorganic Nanoparticles: Synthesis, Applications, and Perspectives. An Overview*; Altavilla, C.; Ciliberto, E., Eds.; CRC Press: New York, 2011; pp 1−17.
(11) Al-Naamani, L.; Dobretsov, S.; Dutta, J. Chitosan-zinc oxide nanoparticle composite coating for active food packaging applications. *Innovative Food Sci. Emerging Technol.* **2016**, *38*, 231−237.
(12) Sankapal, B. R.; Gajare, H. B.; Karade, S. S.; Salunkhe, R. R.; Dubal, D. P. Zinc oxide encapsulated carbon nanotube thin films for energy storage applications. *Electrochim. Acta* **2016**, *192*, 377−384.
(13) Kumar, R.; Al-Dossary, O.; Kumar, G.; Umar, A. Zinc oxide nanostructures for NO 2 gas−sensor applications: A review. *Nano-Micro Lett.* **2015**, *7*, 97−120.
(14) Kumar, S. G.; Rao, K. K. Zinc oxide based photocatalysis: tailoring surface-bulk structure and related interfacial charge carrier dynamics for better environmental applications. *RSC Adv.* **2015**, *5*, 3306−3351.
(15) Hatamie, A.; Khan, A.; Golabi, M.; Turner, A. P.; Beni, V.; Mak, W. C.; Sadollahkhani, A.; Alnoor, H.; Zargar, B.; Bano, S.; et al. Zinc oxide nanostructure-modified textile and its application to biosensing, photocatalysis, and as antibacterial material. *Langmuir* **2015**, *31*, 10913−10921.
(16) Mishra, P. K.; Mishra, H.; Ekielski, A.; Talegaonkar, S.; Vaidya, B. Zinc oxide nanoparticles: a promising nanomaterial for biomedical applications. *Drug Discovery Today* **2017**, *22*, 1825−1834.
(17) Nagajyothi, P.; Cha, S. J.; Yang, I. J.; Sreekanth, T.; Kim, K. J.; Shin, H. M. Antioxidant and anti-inflammatory activities of zinc oxide nanoparticles synthesized using Polygala tenuifolia root extract. *J. Photochem. Photobiol. B* **2015**, *146*, 10−17.
(18) Cai, X.; Luo, Y.; Zhang, W.; Du, D.; Lin, Y. pH-Sensitive ZnO quantum dots−doxorubicin nanoparticles for lung cancer targeted drug delivery. *ACS Appl. Mater. Interfaces* **2016**, *8*, 22442−22450.
(19) Gutha, Y.; Pathak, J. L.; Zhang, W.; Zhang, Y.; Jiao, X. Antibacterial and wound healing properties of chitosan/poly (vinyl alcohol)/zinc oxide beads (CS/PVA/ZnO). *Int. J. Biol. Macromol.* **2017**, *103*, 234−241.
(20) Lai, L.; Zhao, C.; Su, M.; Li, X.; Liu, X.; Jiang, H.; Amatore, C.; Wang, X. In vivo target bio-imaging of Alzheimer's disease by fluorescent zinc oxide nanoclusters. *Biomater. Sci.* **2016**, *4*, 1085−1091.
(21) Periasamy, G.; Karim, A.; Gibrelibanos, M.; Gebremedhin, G. Nutmeg (*Myristica fragrans* Houtt.) Oils. In *Essential Oils in Food Preservation, Flavor and Safety*; Elsevier, 2016; pp 607−616.
(22) Asgarpanah, J.; Kazemivash, N. Phytochemistry and pharmacologic properties of *Myristica fragrans* Hoyutt.: A review. *Afr. J. Biotechnol.* **2012**, *11*, 12787−12793.
(23) Francis, S. K.; James, B.; Varughese, S.; Nair, M. S. Phytochemical investigation on Myristica fragrans stem bark. *Nat. Prod. Res.* **2019**, *33*, 1204−1208.
(24) Barzinjy, A. A.; Hamad, S. M.; Abdulrahman, A. F.; Biro, S. J.; Ghafor, A. A. Biosynthesis, characterization and mechanism of formation of ZnO nanoparticles using Petroselinum crispum leaf extract. *Curr. Org. Synth.* **2020**, *17*, 558−566.
(25) Weil, A. T. Nutmeg as a narcotic. *Econ. Bot.* **1965**, *19*, 194−217.
(26) Chiu, S.; Wang, T.; Belski, M.; Abourashed, E. A., HPLC-guided isolation, purification and characterization of phenylpropanoid and phenolic constituents of nutmeg kernel (*Myristica fragrans*) *Nat. Prod. Commun.* 2016 *11(4) p1934578X1601100416* DOI: 10.1177/1934578X1601100416.
(27) Piras, A.; Rosa, A.; Marongiu, B.; Atzeri, A.; Dessì, M. A.; Falconieri, D.; Porcedda, S. Extraction and separation of volatile and fixed oils from seeds of *Myristica fragrans* by supercritical CO_2: Chemical composition and cytotoxic activity on Caco-2 cancer cells. *J. Food Sci.* **2012**, *77*, C448−C453.
(28) Jan, H.; Shah, M.; Usman, H.; Khan, A.; Muhammad, Z.; Hano, C.; Abbasi, B. H. Biogenic Synthesis and Characterization of Antimicrobial and Anti-parasitic Zinc Oxide (ZnO) Nanoparticles using Aqueous Extracts of the Himalayan Columbine (*Aquilegia pubiflora*). *Front. Mater.* **2020**, *7*, No. 249.
(29) Guilger-Casagrande, M.; de Lima, R. Synthesis of Silver Nanoparticles Mediated by Fungi: A Review. *Front. Bioeng. Biotechnol.* **2019**, *7*, No. 287.
(30) Davis, K.; Yarbrough, R.; Froeschle, M.; White, J.; Rathnayake, H. Band gap engineered zinc oxide nanostructures via a sol−gel synthesis of solvent driven shape-controlled crystal growth. *RSC Adv.* **2019**, *9*, 14638−14648.
(31) Chava, R. K.; Kang, M. Improving the photovoltaic conversion efficiency of ZnO based dye sensitized solar cells by indium doping. *J. Alloys Compd.* **2017**, *692*, 67−76.
(32) Fu, L.; Fu, Z. *Plectranthus amboinicus* leaf extract−assisted biosynthesis of ZnO nanoparticles and their photocatalytic activity. *Ceram. Int.* **2015**, *41*, 2492−2496.
(33) Wang, F.-H.; Chang, C.-L. Effect of substrate temperature on transparent conducting Al and F co-doped ZnO thin films prepared by rf magnetron sputtering. *Appl. Surf. Sci.* **2016**, *370*, 83−91.
(34) Nimbalkar, A. R.; Patil, M. G. Synthesis of ZnO thin film by sol-gel spin coating technique for H_2S gas sensing application. *Physica B* **2017**, *527*, 7−15.
(35) Lu, J.; Batjikh, I.; Hurh, J.; Han, Y.; Ali, H.; Mathiyalagan, R.; Ling, C.; Ahn, J. C.; Yang, D. C. Photocatalytic degradation of methylene blue using biosynthesized zinc oxide nanoparticles from bark extract of *Kalopanax septemlobus*. *Optik* **2019**, *182*, 980−985.
(36) Kim, W. J.; Soshnikova, V.; Markus, J.; Oh, K. H.; Anandapadmanaban, G.; Mathiyalagan, R.; Perez, Z. E. J.; Kim, Y. J.; Yang, D. C. Room temperature synthesis of germanium dioxide nanorods and their in vitro photocatalytic application. *Optik* **2019**, *178*, 664−668.
(37) Zhou, J.; Zhao, F.; Wang, Y.; Zhang, Y.; Yang, L. Size-controlled synthesis of ZnO nanoparticles and their photoluminescence properties. *J. Lumin.* **2007**, *122−123*, 195−197.
(38) Khoshhesab, Z. M.; Sarfaraz, M.; Asadabad, M. A. Preparation of ZnO nanostructures by chemical precipitation method. *Synth. React. Inorg., Met.-Org., Nano-Met. Chem.* **2011**, *41*, 814−819.
(39) Kaskow, I.; Decyk, P.; Sobczak, I. The effect of copper and silver on the properties of Au-ZnO catalyst and its activity in glycerol oxidation. *Appl. Surf. Sci.* **2018**, *444*, 197−207.
(40) Arakha, M.; Saleem, M.; Mallick, B. C.; Jha, S. The effects of interfacial potential on antimicrobial propensity of ZnO nanoparticle. *Sci. Rep.* **2015**, *5*, No. 9578.

https://doi.org/10.1021/acsomega.1c00310
ACS Omega 2021, 6, 9709−9722

(41) Fatimah, I.; Pradita, R. Y.; Nurfalinda, A. Plant extract mediated of ZnO nanoparticles by using ethanol extract of *Mimosa pudica* leaves and coffee powder. *Procedia Eng.* **2016**, *148*, 43−48.
(42) Rajiv, P.; Rajeshwari, S.; Venckatesh, R. Bio-Fabrication of zinc oxide nanoparticles using leaf extract of *Parthenium hysterophorus* L. and its size-dependent antifungal activity against plant fungal pathogens. *Spectrochim. Acta, Part A* **2013**, *112*, 384−387.
(43) Pillai, A. M.; Sivasankarapillai, V. S.; Rahdar, A.; Joseph, J.; Sadeghfar, F.; Rajesh, K.; Kyzas, G. Z.; et al. Green synthesis and characterization of zinc oxide nanoparticles with antibacterial and antifungal activity. *J. Mol. Struct.* **2020**, *1211*, No. 128107.
(44) Modena, M. M.; Rühle, B.; Burg, T. P.; Wuttke, S. Nanoparticle Characterization: Nanoparticle Characterization: What to Measure? *Adv. Mater.* **2019**, *31*, No. 1970226.
(45) Vimala, K.; Sundarraj, S.; Paulpandi, M.; Vengatesan, S.; Kannan, S. Green synthesized doxorubicin loaded zinc oxide nanoparticles regulates the Bax and Bcl-2 expression in breast and colon carcinoma. *Process Biochem.* **2014**, *49*, 160−172.
(46) Lynch, I.; Dawson, K. A. Protein-nanoparticle interactions. *Nano Today* **2008**, *3*, 40−47.
(47) Romero, C. D.; Chopin, S. F.; Buck, G.; Martinez, E.; Garcia, M.; Bixby, L. Antibacterial properties of common herbal remedies of the southwest. *J. Ethnopharmacol.* **2005**, *99*, 253−257.
(48) Boucher, H. W.; Talbot, G. H.; Bradley, J. S.; Edwards, J. E.; Gilbert, D.; Rice, L. B.; Scheld, M.; Spellberg, B.; Bartlett, J. Bad bugs, no drugs: no ESKAPE! An update from the Infectious Diseases Society of America. *Clin. Infect. Dis.* **2009**, *48*, 1−12.
(49) Talbot, G. H.; Bradley, J.; Edwards, J. E., Jr.; Gilbert, D.; Scheld, M.; Bartlett, J. G. Bad bugs need drugs: an update on the development pipeline from the Antimicrobial Availability Task Force of the Infectious Diseases Society of America. *Clin. Infect. Dis.* **2006**, *42*, 657−668.
(50) Rajeshkumar, S.; Menon, S.; Kumar, S. V.; Tambuwala, M. M.; Bakshi, H. A.; Mehta, M.; Satija, S.; Gupta, G.; Chellappan, D. K.; Thangavelu, L. Antibacterial and antioxidant potential of biosynthesized copper nanoparticles mediated through *Cissus arnotiana* plant extract. *J. Photochem. Photobiol. B* **2019**, *197*, No. 111531.
(51) Faisal, S.; Khan, M. A.; Jan, H.; Shah, S. A.; Shah, S.; Rizwan, M.; Ullah, W.; Akbar, M. T. Edible mushroom (*Flammulina velutipes*) as biosource for silver nanoparticles: from synthesis to diverse biomedical and environmental applications. *Nanotechnology* **2020**, *32*, No. 065101.
(52) Awwad, A. M.; Amer, M. W.; Salem, N. M.; Abdeen, A. O. Green synthesis of zinc oxide nanoparticles (ZnO-NPs) using *Ailanthus altissima* fruit extracts and antibacterial activity. *Chem. Int.* **2020**, *6*, 151−159.
(53) Roux, P. P.; Blenis, J. ERK and p38 MAPK-activated protein kinases: a family of protein kinases with diverse biological functions. *Microbiol. Mol. Biol. Rev.* **2004**, *68*, 320−344.
(54) Pathania, D.; Millard, M.; Neamati, N. Opportunities in discovery and delivery of anticancer drugs targeting mitochondria and cancer cell metabolism. *Adv. Drug Delivery Rev.* **2009**, *61*, 1250−1275.
(55) Mohamed, H. E. A.; Afridi, S.; Khalil, A. T.; Zia, D.; Shinwari, Z. K.; Dhlamini, M. S.; Maaza, M. Structural, morphological and biological features of ZnO nanoparticles using *Hyphaene thebaica* (L.) Mart. fruits. *J. Inorg. Organomet. Polym. Mater.* **2020**, *30*, 3241−3254.
(56) Nair, A.; Jayakumari, C.; Jabbar, P.; Jayakumar, R.; Raizada, N.; Gopi, A.; George, G. S.; Seena, T. Prevalence and associations of hypothyroidism in Indian patients with type 2 diabetes mellitus. *J. Thyroid Res.* **2018**, *2018*, No. 5386129.
(57) Aynalem, S. B.; Zeleke, A. J. Prevalence of diabetes mellitus and its risk factors among individuals aged 15 years and above in Mizan-Aman town, Southwest Ethiopia, 2016: a cross sectional study. *Int. J. Endocrinol.* **2018**, *2018*, No. 9317987.
(58) Thiruvengadam, M.; Chung, I.-M.; Gomathi, T.; Ansari, M. A.; Khanna, V. G.; Babu, V.; Rajakumar, G. Synthesis, characterization and pharmacological potential of green synthesized copper nanoparticles. *Bioprocess Biosyst. Eng.* **2019**, *42*, 1769−1777.
(59) Vasudeo, K.; Pramod, K. Biosynthesis of nickel nanoparticles using leaf extract of coriander. *Biotechnology* **2016**, *12*, 1−6.
(60) Sergiev, I.; Todorova, D.; Shopova, E.; Jankauskiene, J.; Jankovska-Bortkevič, E.; Jurkonienė, S. Exogenous auxin type compounds amend PEG-induced physiological responses of pea plants. *Sci. Hortic.* **2019**, *248*, 200−205.
(61) Mohamed, H. I.; Akladious, S. A. Changes in antioxidants potential, secondary metabolites and plant hormones induced by different fungicides treatment in cotton plants. *Pestic. Biochem. Physiol.* **2017**, *142*, 117−122.
(62) Rehman, M.; Ullah, S.; Bao, Y.; Wang, B.; Peng, D.; Liu, L. Light-emitting diodes: whether an efficient source of light for indoor plants? *Environ. Sci. Pollut. Res.* **2017**, *24*, 24743−24752.
(63) Prieto, M.; Curran, T. P.; Gowen, A.; Vázquez, J. A. An efficient methodology for quantification of synergy and antagonism in single electron transfer antioxidant assays. *Food Res. Int.* **2015**, *67*, 284−298.
(64) Stanisavljević, N.; Bajić, S. S.; Jovanović, Ž.; Matić, I.; Tolinački, M.; Popović, D.; Popović, N.; Terzić-Vidojević, A.; Golić, N.; Beškoski, V.; et al. Antioxidant and antiproliferative activity of *Allium ursinum* and their associated microbiota during simulated in vitro digestion in the presence of food matrix. *Front. Microbiol.* **2020**, *11*, No. 601616.
(65) Skonieczna, M.; Hudy, D. Biological Activity of Silver Nanoparticles and Their Applications in Anticancer Therapy. In *Silver Nanoparticles: Fabrication, Characterization and Applications. Intechopen* 2018; p 131.
(66) Ul-Haq, I.; Ullah, N.; Bibi, G.; Kanwal, S.; Ahmad, M. S.; Mirza, B. Antioxidant and cytotoxic activities and phytochemical analysis of *Euphorbia wallichii* root extract and its fractions. *Iran. J. Pharm. Res.* **2012**, *11*, 241.
(67) Khalil, A. T.; Ovais, M.; Ullah, I.; Ali, M.; Shinwari, Z. K.; Hassan, D.; Maaza, M. *Sageretia thea* (Osbeck.) modulated biosynthesis of NiO nanoparticles and their in vitro pharmacognostic, antioxidant and cytotoxic potential. *Artif. Cells, Nanomed., Biotechnol.* **2018**, *46*, 838−852.
(68) Akbari, M.; Oryan, A.; Hatam, G. Application of nanotechnology in treatment of leishmaniasis: A Review. *Acta Trop.* **2017**, *172*, 86−90.
(69) Jebali, A.; Kazemi, B. Nano-based antileishmanial agents: a toxicological study on nanoparticles for future treatment of cutaneous leishmaniasis. *Toxicol. In Vitro* **2013**, *27*, 1896−1904.
(70) Jan, H.; Khan, M. A.; Usman, H.; Shah, M.; Ansir, R.; Faisal, S.; Ullah, N.; Rahman, L. The *Aquilegia pubiflora* (Himalayan columbine) mediated synthesis of nanoceria for diverse biomedical applications. *RSC Adv.* **2020**, *10*, 19219−19231.
(71) World Health Organization. *Comprehensive Guideline for Prevention and Control of Dengue and Dengue Haemorrhagic Fever*, 2011.
(72) Johnson, N.; de Marco, M. F.; Giovannini, A.; Ippoliti, C.; Danzetta, M. L.; Svartz, G.; Erster, O.; Groschup, M. H.; Ziegler, U.; Mirazimi, A.; et al. Emerging mosquito-borne threats and the response from European and eastern Mediterranean countries. *Int. J. Environ. Res. Public Health* **2018**, *15*, No. 2775.
(73) Brix, K. V.; Cardwell, R. D.; Adams, W. J. Chronic toxicity of arsenic to the Great Salt Lake brine shrimp, *Artemia franciscana*. *Ecotoxicol. Environ. Saf.* **2003**, *54*, 169−175.
(74) Ozkan, Y.; Altinok, I.; Ilhan, H.; Sokmen, M. Determination of TiO_2 and $AgTiO_2$ nanoparticles in *Artemia salina*: toxicity, morphological changes, uptake and depuration. *Bull. Environ. Contam. Toxicol.* **2016**, *96*, 36−42.
(75) Klaine, S. J.; Alvarez, P. J.; Batley, G. E.; Fernandes, T. F.; Handy, R. D.; Lyon, D. Y.; Mahendra, S.; McLaughlin, M. J.; Lead, J. R. Nanomaterials in the environment: behavior, fate, bioavailability, and effects. *Environ. Toxicol. Chem.* **2008**, *27*, 1825−1851.
(76) Khoshnood, R.; Jaafarzadeh, N.; Jamili, S.; Farshchi, P.; Taghavi, L. Acute toxicity of TiO_2, CuO and ZnO nanoparticles in brine shrimp, *Artemia franciscana*. *Iran. J. Fish. Sci.* **2017**, *16*, 1287−1296.

https://doi.org/10.1021/acsomega.1c00310
ACS Omega 2021, 6, 9709−9722

(77) Nasar, M. Q.; Khalil, A. T.; Ali, M.; Shah, M.; Ayaz, M.; Shinwari, Z. K. Phytochemical analysis, Ephedra Procera CA Mey. Mediated green synthesis of silver nanoparticles, their cytotoxic and antimicrobial potentials. *Medicina* **2019**, *55*, No. 369.
(78) Sajadi, S. M.; Kolo, K.; Hamad, S. M.; Mahmud, S. A.; Barzinjy, A. A.; Hussein, S. M. Green Synthesis of the Ag/Bentonite Nanocomposite UsingEuphorbia larica Extract: A Reusable Catalyst for Efficient Reduction of Nitro Compounds and Organic Dyes. *ChemistrySelect* **2018**, *3*, 12274−12280.
(79) Su, Y.; Yang, Y.; Zhang, H.; Xie, Y.; Wu, Z.; Jiang, Y.; Fukata, N.; Bando, Y.; Wang, Z. L. Enhanced photodegradation of methyl orange with TiO_2 nanoparticles using a triboelectric nanogenerator. *Nanotechnology* **2013**, *24*, No. 295401.
(80) Holzwarth, U.; Gibson, N. The Scherrer equation versus the Debye−Scherrer equation. *Nat. Nanotechnol.* **2011**, *6*, 534.
(81) Barzinjy, A.; Mustafa, S.; Ismael, H. Characterization of ZnO NPs prepared from green synthesis using Euphorbia Petiolata leaves. *Eurasian J. Sci. Eng.* **2019**, *4*, 74−83.
(82) Morais, M.; Namouni, F. Asteroids in retrograde resonance with Jupiter and Saturn. *Mon. Not. R. Astron. Soc.: Lett.* **2013**, *436*, L30−L34.
(83) Shah, M.; Nawaz, S.; Jan, H.; Uddin, N.; Ali, A.; Anjum, S.; Giglioli-Guivarc'h, N.; Hano, C.; Abbasi, B. H. Synthesis of bio-mediated silver nanoparticles from *Silybum marianum* and their biological and clinical activities. *Mater. Sci. Eng. C* **2020**, *112*, No. 110889.
(84) Faisal, S.; Khan, M. A.; Jan, H.; Shah, S. A.; Abdullah, A.; Shah, S.; Rizwan, M.; Ullah, W.; Akbar, M. T.; Redaina, R. Edible Mushroom (*Flammulina velutipes*) as Biosource for Silver Nano-particles: From Synthesis to Diverse Biomedical and Environmental Applications *Nanotechnology* 2020 *32* No 6: (065101)6 DOI: 10.1088/1361-6528/abc2eb.
(85) Usman, H.; Ullah, M. A.; Jan, H.; Siddiquah, A.; Drouet, S.; Anjum, S.; Giglioli-Guviarc'h, N.; Hano, C.; Abbasi, B. H. Interactive Effects of wide-spectrum monochromatic lights on phytochemical production, antioxidant and biological activities of *Solanum xanthocarpum* callus cultures. *Molecules* **2020**, *25*, No. 2201.
(86) Nazir, S.; Jan, H.; Tungmunnithum, D.; Drouet, S.; Zia, M.; Hano, C.; Abbasi, B. H. Callus Culture of Thai Basil Is an Effective Biological System for the Production of Antioxidants. *Molecules* **2020**, *25*, No. 4859.
(87) Abdel-Aziz, H. M.; Rizwan, M. Chemically synthesized silver nanoparticles induced physio-chemical and chloroplast ultrastructural changes in broad bean seedlings. *Chemosphere* **2019**, *235*, 1066−1072.
(88) Soflaei, S.; Dalimi, A.; Abdoli, A.; Kamali, M.; Nasiri, V.; Shakibaie, M.; Tat, M. Anti-leishmanial activities of selenium nanoparticles and selenium dioxide on *Leishmania infantum*. *Comp. Clin. Pathol.* **2014**, *23*, 15−20.
(89) Gerberg, E. J.; Barnard, D. R.; Ward, R. A. *Manual for Mosquito Rearing and Experimental Techniques*; American Mosquito Control Association, Inc., 1994.
(90) Elango, G.; Roopan, S. M.; Al-Dhabi, N. A.; Arasu, M. V.; Dhamodaran, K. I.; Elumalai, K. Coir mediated instant synthesis of Ni-Pd nanoparticles and its significance over larvicidal, pesticidal and ovicidal activities. *J. Mol. Liq.* **2016**, *223*, 1249−1255.
(91) Kumar, K. P.; Paul, W.; Sharma, C. P. Green synthesis of gold nanoparticles with Zingiber officinale extract: characterization and blood compatibility. *Process Biochem.* **2011**, *46*, 2007−2013.
(92) Nasrollahzadeh, M.; Sajjadi, M.; Maham, M.; Sajadi, S. M.; Barzinjy, A. A. Biosynthesis of the palladium/sodium borosilicate nanocomposite using *Euphorbia milii* extract and evaluation of its catalytic activity in the reduction of chromium (VI), nitro compounds and organic dyes. *Mater. Res. Bull.* **2018**, *102*, 24−35.

NOTE ADDED AFTER ASAP PUBLICATION

This paper was published on the Web on March 30, 2021. Author name Wajid Ullah was changed to Wajidullah. The corrected version was reposted on March 31, 2021.

https://doi.org/10.1021/acsomega.1c00310
ACS Omega 2021, 6, 9709−9722